

Actin Polymerization Kinetics, Cap Structure and Fluctuations

Ben O'Shaughnessy[†]*, Dimitrios Vavylonis[†], and Qingbo Yang[‡]

Departments of [†]Chemical Engineering and [‡]Physics, Columbia University, New York, NY 10027, USA

October 15, 2019

Polymerization of actin proteins into dynamic structures is essential to eukaryotic cell life. This has motivated a large body of in vitro experiments measuring polymerization kinetics of individual filaments. Here we model these kinetics, accounting for all relevant steps revealed by experiment: polymerization, depolymerization, random ATP hydrolysis and release of phosphate (Pi). We quantitatively relate filament growth rates to the dynamics of ATP-actin and ADP-Pi-actin caps which develop at filament ends in steady state. At the critical concentration there is a short ATP cap and a long fluctuation-stabilized ADP-Pi-actin cap, suggesting the difference in critical concentrations at the barbed and pointed filament ends may depend on differences between the ATP-actin and ADP-Pi-actin species. Fluctuations in filament lengths are described by the length diffusion coefficient, D , which exhibits a pronounced peak near the barbed end critical concentration due to filaments alternating between capped and uncapped states, a mild version of the dynamical instability leading to catastrophes in microtubule polymerization. Recently Fujiwara et al. [*Nature Cell Biol.* (2002) 4, 666] observed large steady state filament length fluctuations, provoking speculation that growth may proceed by oligomeric rather than monomeric on-off events. Our results suggest the observed fluctuations may be an intrinsic feature of single-monomer growth kinetics.

The tendency of actin protein to spontaneously polymerize into rapidly growing filaments is fundamental to the life of eukaryotic cells. Cell motility, cell division, and phagocytosis are examples of processes exploiting the dynamic character of actin structures composed of filaments [1]. The regulation of filament growth processes can lead to well-defined structures and coordinated function. For example, in combination with branching, capping, and depolymerizing proteins, actin self-assembles into controlled dynamic cross-linked networks forming the dynamic core of the lamellipodium in locomoting cells [2].

These complex cellular actin-based systems exhibit multiple superposed mechanisms. This has inspired a large body of in vitro work aiming to unravel these mechanisms and pin down rate constants for the constituent processes in purified systems [3]. An important class of experiments entails blocking one filament end with a capping protein and measuring growth rate at the other end as a function of actin monomer concentration [4–11]. From these and other in vitro studies using various labeling techniques the following picture has emerged of filament growth kinetics in the presence of ATP (see fig. 1). (i) Monomers are added to a growing filament end as ATP-actin. (ii) Rapidly, the ATP is then hydrolyzed to ADP and phosphate (Pi), both remaining bound to the monomer host (ADP-Pi-actin) [4, 9, 12–17]. A rate of 0.3s^{-1} was reported in ref. 17 in the presence of Mg, assuming random hydrolysis uninfluenced by neighboring monomers. (iii) After a long

delay phosphate release into solution occurs, generating ADP-actin [18–20]. Reported release rates are in the range $0.002 - 0.006\text{s}^{-1}$ [2, 18–20].

A typical filament in a growth rate experiment is thousands of monomer units in length and thus consists mainly of ADP-actin. Hence the picture which emerges is of a long ADP-actin filament with a complex 3-state *cap* region at the filament end [3] (see fig. 1). A major goal of this report is to establish the composition and kinetics of the cap, and how these determine growth rates and measurable length fluctuations. This is important in the context of cellular processes: the monomer composition in actin filaments is thought to regulate actin-binding proteins in a timely and spatially organized way [2]. For example, it has been suggested that rates of branching generated by the Arp2/3 protein complex and/or debranching processes may depend on which of the 3 monomer species is involved, ATP-actin, ADP-Pi-actin or ADP-actin [21, 22]. Phosphate release is proposed to act as a timer for the action of the depolymerizing/severing protein ADF/cofilin which preferentially attacks ADP-actin [2].

Our aim in this report is to establish theoretically the quantitative implications of the currently held picture of actin polymerization. We will argue that some features of filament kinetics are universal, whereas others depend on detailed numerical parameter values. Previous theoretical works addressed growth rates before the important process of phosphate release was established [23–25]. To date there has been no theoretical analysis of single filament growth rates and fluctuations rigorously accounting for the processes (i)-(iii) above. A related theoretical work [26] has addressed steady state filament compositions (see discussion).

The cap has important consequences for the growth rate j as a function of ATP-actin concentration, c . Measured $j(c)$ curves, such as those in fig. 2, are strikingly non-linear near the critical concentration, c_{crit} , at which mean growth rate vanishes. These become almost linear in excess phosphate studies, where presumably the ADP-actin species is no longer involved [11]. The complexity of the cap structure and dynamics also underlies the values of c_{crit} at the fast-growing “barbed” end and slow-growing “pointed” end of the polar actin filament. It is well known that in general these are different since detailed balance cannot be invoked for these non-equilibrium polymers [25]. Our work explores how cap properties determine the difference in c_{crit} values.

The major experimental focus has been mean growth rates, $j(c)$. However, equally revealing are *fluctuations* about the mean whose measurement can expose features of the dynamical processes occurring at filament ends unavailable from $j(c)$. These fluctuations are characterized by a “length diffusivity” D measuring the spread in filament lengths (see fig. 1(b)) similarly to simple one dimensional Fickian diffusion: after time t , the root mean square fluctuation in filament length is $(2Dt)^{1/2}$ about the mean value $j(c)t$. Using single filament microscopy, Fujiwara et al. [27] recently measured unexpect-

*To whom correspondence should be addressed. E-mail: bo8@columbia.edu

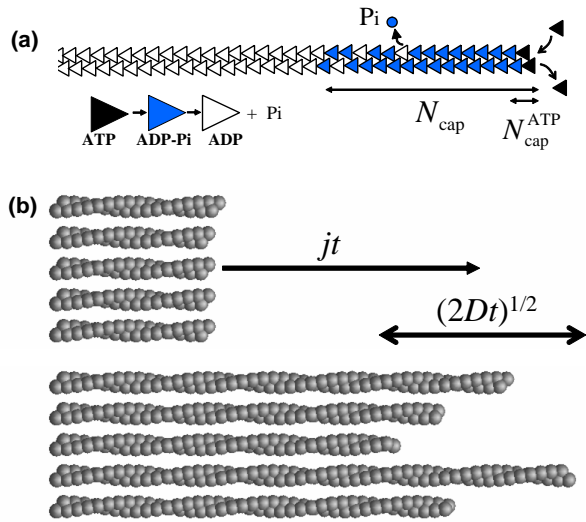


Figure 1: (a) Schematic of the 3-species cap at the barbed end of a long actin filament. Near the critical concentration we find a fluctuation-induced cap of $N_{\text{cap}} \approx 25$ monomers, with a short ATP-actin component, $N_{\text{cap}}^{\text{ATP}}$ of order unity. (b) Mean growth rate and fluctuations: in time t the average number of monomers added to a filament end is jt , with a spread of $(2Dt)^{1/2}$ about this value.

edly high values of this diffusivity in steady state conditions, $D \approx 25 - 29 \text{ mon}^2/\text{s}$. This should be compared with what would be expected of an equilibrium polymerization involving the measured on/off rates of order $1 \text{ mon}/\text{s}$, which would lead to $D \approx 1 \text{ mon}^2/\text{s}$ [25, 27–29]. Two alternative explanations were proposed [27, 30]. (i) Fluctuations arise from “dynamical instability” due to stochastic cap loss episodes. This would be a far milder version of the “catastrophes” in microtubule polymerization. (ii) Filament polymerization proceeds by addition and subtraction of *oligomeric* actin segments. Explanation (ii), if correct, would constitute a radical departure from the accepted picture of filament growth kinetics involving single monomer addition events. A major focus of this report is to calculate the concentration-dependent length diffusivity, $D(c)$, assuming the monomer-by-monomer addition picture is valid.

We consider the initial condition realized in the experiments of fig. 2 where long pre-formed ADP-actin filaments (seeds) are diluted at $t = 0$ in a buffer of *fixed* actin concentration c and excess ATP. The analysis is equally applicable to either the barbed or pointed end, the other end assumed blocked; specializing to a given end simply requires inputting the numerical parameters appropriate for that end. Our results apply to very dilute filaments where only ATP-actin is assumed to add to filaments since (i) monomers bind ATP more strongly than ADP [31], and (ii) depolymerized ADP-actin or ADP-Pi-actin has enough time to exchange its nucleotide for ATP before repolymerization. An important issue is the nature of the ATP hydrolysis mechanism. The experiments of refs. 15, 16 support a random mechanism, though others have favored a cooperative vectorial mechanism occurring at the interface between ADP-Pi-actin and ATP-actin with rate 13.6 s^{-1} [14, 23]. In this study, random hydrolysis is assumed throughout.

Cap Structure and the Importance of Fluctuations

Before calculating $j(c)$ and $D(c)$ exactly, we will use scaling arguments to estimate the cap structure whose dependence on actin concentration c will help in understanding how j and D

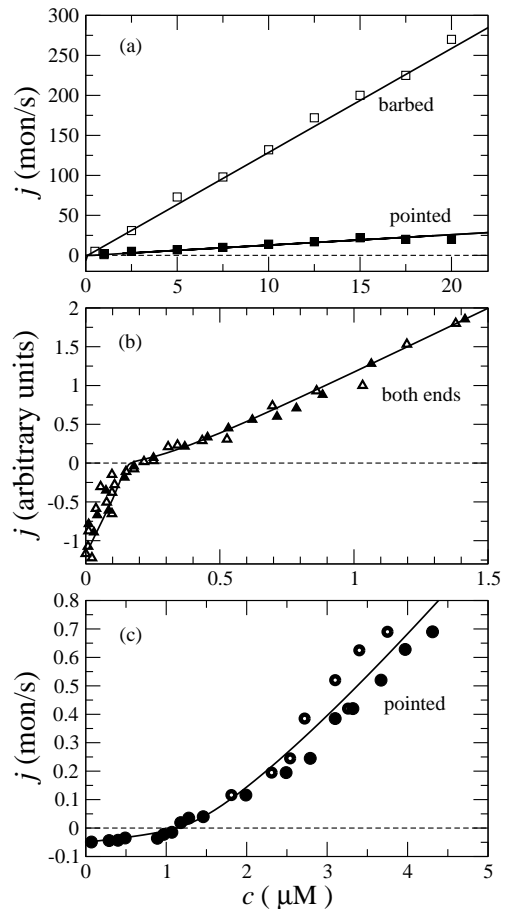


Figure 2: Growth rates $j(c)$ versus concentration. Experiments performed in ATP, KCl, and MgCl_2 . Theoretical fits using one body model, solid curves. (a) Electron microscopy measurements taken from fig. 3 of ref. 6. Parameters for theory: barbed end, $k_{\text{T}}^+ = 13 \mu\text{M}^{-1} \text{ s}^{-1}$, $v_{\text{D}}^- = 7.2 \text{ s}^{-1}$, $v_{\text{T}}^- = 1.4 \text{ s}^{-1}$, $v_{\text{P}}^- = .8 \text{ s}^{-1}$; pointed end, same as thin curve in fig. 3(a). (b) Fluorescence data taken from fig. 1 of ref. 9, simultaneous growth at both ends. Theory (barbed end only): $k_{\text{T}}^+ = 10 \mu\text{M}^{-1} \text{ s}^{-1}$, $v_{\text{D}}^- = 7 \text{ s}^{-1}$, $v_{\text{T}}^- = 3.1 \text{ s}^{-1}$, and $v_{\text{P}}^- = .4 \text{ s}^{-1}$, scaled to fit data. (c) Pointed end fluorescence data from fig. 1 of ref. 10. Theory: $k_{\text{T}}^+ = 0.36 \mu\text{M}^{-1} \text{ s}^{-1}$, $v_{\text{D}}^- = .05 \text{ s}^{-1}$, $v_{\text{T}}^- = 1 \text{ s}^{-1}$, and $v_{\text{P}}^- = .25 \text{ s}^{-1}$. NB: almost linear curves were obtained for pointed end in refs. 7, 8 in different buffers.

depend on c . Because hydrolysis is fast whereas phosphate release is slow one anticipates a short ATP-actin segment of length $N_{\text{cap}}^{\text{ATP}}$ at the filament end, while the total cap length N_{cap} may be much greater (see fig. 1(a)).

To determine how $N_{\text{cap}}^{\text{ATP}}$ and N_{cap} depend on c , it is helpful to digress briefly to analyze an exactly solvable 2-species model, defined by two assumptions: (A) ATP-actin and ADP-Pi-actin are identical species and (B) phosphate is never released. The motivation for (B) is that the actual phosphate release rate is much less than typical monomer on/off rates. Below c_{crit} , this model generates a steady state ATP-actin cap at the end of the ADP-actin core as follows. Now on average the cap is shrinking with a negative velocity $v_{\text{cap}} = k_{\text{T}}^+ c - v_{\text{T}}^-$, where k_{T}^+ and v_{T}^- are the ATP-actin on and off rate constants. Equally important, however, are *fluctuations* in cap length: the cap tip performs a 1D random walk with diffusivity $D_{\text{cap}} = (k_{\text{T}}^+ c + v_{\text{T}}^-)/2$ due to the randomness of monomer addition/subtraction events [28, 29]. For small times, diffusivity dominates and of order $(D_{\text{cap}} t)^{1/2}$ units add to the cap. For

times less than the cap turnover time t_{cap} , this is much bigger than the number of units wiped out by coherent shrinkage, $v_{\text{cap}}t$. The cap lifetime t_{cap} is the time when the shrinkage just catches up, $v_{\text{cap}}t_{\text{cap}} = (D_{\text{cap}}t_{\text{cap}})^{1/2}$. Hence the cap length is

$$N_{\text{cap}} = v_{\text{cap}}t_{\text{cap}} = c_{\text{crit}}/(c_{\text{crit}} - c), \quad (c < c_{\text{crit}}) \quad (1)$$

where $c_{\text{crit}} = v_{\text{T}}^-/k_{\text{T}}^+$. A rigorous calculation shows that this result is exact as the concentration approaches c_{crit} from below, with prefactor unity as displayed.

Now one might have guessed that below c_{crit} there would be no cap at all, since the filament is shrinking into its ADP core. This is quite wrong, as indicated by eq. (1), because it neglects fluctuations: there is a *fluctuation-stabilized* cap, becoming infinitely long as c_{crit} is approached since net growth rate is becoming tiny and increasingly overwhelmed by cap length diffusion. Above c_{crit} the cap is of course infinite, since ATP-actin monomers add to the ADP-actin core without bound.

The simplified model captures essential features of the real growth kinetics. As we now undo assumptions (A) and (B), it will be seen that although caps are never infinite, the characteristic of very long caps near c_{crit} remains. We first undo assumption (A), i. e. ATP-actin and ADP-Pi-actin are now allowed to have different rate constants, as in reality. In this case it can be shown that eq. (1) in fact remains valid, as follows. Since on/off rates close to c_{crit} are comparable to the rate of hydrolysis, thus the length of the ATP-actin segment $N_{\text{cap}}^{\text{ATP}}$ is of order unity. But this is much smaller than the fluctuation-induced size of the entire cap, N_{cap} . Hence the tip has a well defined growth rate, $\tilde{v}_{\text{cap}}(c)$, representing a weighted average of growth rates summed over all possible states of the short ATP-actin segment on top of the long ADP-Pi-actin segment. Since \tilde{v}_{cap} is a smooth function of c , near the critical concentration one has $\tilde{v}_{\text{cap}} = \tilde{k}^+(c - c_{\text{crit}})$ where \tilde{k}^+ is a renormalized rate constant different from k_{T}^+ . (Note the critical concentration c_{crit} is also modified from its value $v_{\text{T}}^-/k_{\text{T}}^+$ in the simplified model.) Similar remarks apply to the tip diffusivity, which is renormalized to $\tilde{D}_{\text{cap}}(c)$ and is similarly a smooth function near c_{crit} where its magnitude is of order $\tilde{k}^+c_{\text{crit}}$. Repeating the earlier arguments, but replacing $v_{\text{cap}} \rightarrow \tilde{v}_{\text{cap}}$ and $D_{\text{cap}} \rightarrow \tilde{D}_{\text{cap}}$, one recovers eq. (1) but with a modified prefactor of order unity.

Finally, assumption (B) must be undone. How is eq. (1) modified by non-zero phosphate release rate, r_{Pi} ? Clearly, the ADP-Pi segment is now always finite and spotted with ADP-actin units (see fig. 1(a)). Its precise morphology is determined by a comparison of the phosphate release time with the residence times of monomers at different cap locations. Near c_{crit} tip diffusion dominates coherent shrinkage, so all monomers within a distance $N_{\text{cap}}^{\text{crit}} \approx (2\tilde{D}_{\text{cap}}/r_{\text{Pi}})^{1/2}$ of the tip will have been replaced by new ones before they had a chance to release their phosphate. By contrast, monomers further away from the tip had time for phosphate release before depolymerizing. It follows that the cap can never become longer than $N_{\text{cap}}^{\text{crit}}$. Equating this to the cap length of eq. (1) identifies the concentration where this upper bound is reached: phosphate release limits the cap size for concentrations within a range Δc about c_{crit} , where $\Delta c/c_{\text{crit}} \approx 1/N_{\text{cap}}^{\text{crit}}$. Now far above c_{crit} filaments grow at the same rate as the cap tip, i. e. $j = \tilde{v}_{\text{cap}}$ so phosphate release simply follows the tip with a lag of $N_{\text{cap}} \approx j/r_{\text{Pi}}$ monomers. In summary, there are several regimes for the cap

size:

$$N_{\text{cap}} \approx \begin{cases} c_{\text{crit}}/(c_{\text{crit}} - c) & (c < c_{\text{crit}} - \Delta c) \\ (2\tilde{D}_{\text{cap}}/r_{\text{Pi}})^{1/2} & (|c - c_{\text{crit}}| < \Delta c) \\ j(c)/r_{\text{Pi}} & (c > c_{\text{crit}} + \Delta c) \end{cases} \quad (2)$$

It can be shown that an additional effect of phosphate release is a shift of c_{crit} itself by an amount $\delta c_{\text{crit}} \approx 1/N_{\text{cap}}^{\text{crit}}$. For brevity's sake, this will be discussed in a forthcoming work. (An implication of this shift is that the variable c_{crit} as it appears in eq. (2) is slightly different to the actual c_{crit} value defined by $j(c_{\text{crit}}) = 0$. For the barbed end, in practice $N_{\text{cap}}^{\text{crit}} \approx 25$ leading to a 4% relative difference.)

Eq. (2) describes the size of the composite ATP-actin/ADP-Pi-actin cap. How long is the ATP-actin segment? This becomes large for concentrations above $c^* \approx (r_{\text{H}} + v_{\text{T}}^-)/k_{\text{T}}^+$, when polymerization rates exceed both the hydrolysis rate r_{H} and the depolymerization rate. Above this threshold the interface between ADP-Pi-actin and ATP-actin follows the tip with a lag of $(k_{\text{T}}^+c - v_{\text{T}}^-)/r_{\text{H}}$ monomers. Thus

$$N_{\text{cap}}^{\text{ATP}} \approx (k_{\text{T}}^+c - v_{\text{T}}^-)/r_{\text{H}}, \quad (c > c^*) \quad (3)$$

For concentrations below c^* , the ATP-actin cap size is of order unity or less. Eqs. (2) and (3) describe the scaling structure of the cap to within order unity prefactors which are in general complex functions of the rate constants. They define 4 regions of behavior, I-IV (see fig. 3).

Fig. 3(b) shows exact numerical calculations of cap sizes (described below) using experimental values of barbed end rate constants. Hydrolysis and phosphate release rates were $r_{\text{H}} = 0.3\text{s}^{-1}$ and $r_{\text{Pi}} = 0.004\text{s}^{-1}$ while as reported in ref. 6 in the presence of 50mM KCl and 1mM MgCl₂, $k_{\text{T}}^+ = 11.6\mu\text{M}^{-1}\text{s}^{-1}$, $v_{\text{T}}^- = 1.4\text{s}^{-1}$ and the depolymerization rate of ADP-actin was taken as $v_{\text{D}}^- = 7.2\text{s}^{-1}$. At present there is no direct measurement of the depolymerization rate of ADP-Pi-actin, v_{P}^- , but $j(c)$ measurements with excess phosphate [11] show the sum of the ADP-Pi-actin off rates at both ends is a few times smaller than v_{D}^- ; we have chosen $v_{\text{P}}^- = 0.8\text{s}^{-1}$. For these values, our calculations for $j(c)$ (see below) indicate $c_{\text{crit}} = 0.105\mu\text{M}$.

From fig. 3(b), the cap size at the critical concentration is $N_{\text{cap}}^{\text{crit}} \approx 25$, giving a theoretical value for the critical window half width $\Delta c \approx 0.004\mu\text{M}$. In this domain (region II in fig. 3) $17 \lesssim N_{\text{cap}}^{\text{crit}} \lesssim 35$. Estimating $\tilde{D}_{\text{cap}} \approx k_{\text{T}}^+c_{\text{crit}} = 1.22\text{s}^{-1}$, the theoretically predicted critical region cap length (eq. (2)) is $N_{\text{cap}}^{\text{crit}} = (2\tilde{D}_{\text{cap}}/r_{\text{Pi}})^{1/2} \approx 25$ in agreement with numerics. (This value should not be taken too seriously, however, due to prefactor uncertainties in scaling arguments.) The observed behavior for $c < c_{\text{crit}} - \Delta c$ (region I) is consistent with eq. (2), with cap size rapidly increasing as c_{crit} is approached. Note also that as predicted in eq. (3) the ATP-actin segment length is less than or order unity below $c^* = 0.147\mu\text{M}$, rapidly increasing thereafter in region IV ($c > c^*$).

Barbed End: Growth Rate Curve, $j(c)$

How is the behavior of growth rate $j(c)$ correlated to these regions I-IV of distinct cap structure and dynamics? Fig. 3(a) shows exact numerical results for barbed end growth, using identical parameters to those of fig. 3(b). The methods of solution are described below. A noticeable feature is that the slopes in regions I and IV are very different. This can be understood as follows. In region IV ($c > c^*$) the ATP-actin segment is

long and hides the remaining ADP-Pi-actin portion of the cap, so $j \approx k_T^+ c - v_T^-$ has simple linear form and slope k_T^+ , approximately behaving as if ATP-actin were the only species involved. On the other hand in region I the growth rate reflects rapidly increasing cap length as concentration increases (see fig. 3(b)). Filament length change is now generated by capless episodes, when the ADP-actin core is exposed and the filament shrinks with velocity v_D^- (the cap being in steady state does not on average contribute). Thus $j = -v_D^- p_{\text{core}}$ where $p_{\text{core}} \approx 1/N_{\text{cap}}$ is the probability the cap length vanishes, assuming a broad distribution of cap lengths with mean N_{cap} . Using eq. (2), this gives $j \approx v_D^- (c_{\text{crit}} - c)/c_{\text{crit}}$ with slope v_D^-/c_{crit} . Since v_D^- is large, this is a much larger slope than in region IV.

Region III is similar to IV, in that the ADP core is covered and so the slope is small. However, since $c < c^*$ the ATP-actin segment at the filament tip is order one or less in length. This leads in general to non-linear behavior, reflecting the changing composition at the cap tip as concentration increases towards c^* . For these parameter values, the non-linearity in fig. 3(a) is small. Finally, the critical region II is a narrow transition region from large to small slope. Theoretically and numerically, we found its width Δc was approximately 4% of the critical concentration, a consequence of the small phosphate release rate.

Methods of solution. To calculate the filament growth rates in fig. 3(a), one is faced with the formidable task of obtaining the steady state probability distribution of all possible actin monomer sequences along the filament. Unless one resorts to uncontrolled preaveraging approximations, a full analytical or numerical solution is intractable: there are 3 possible states per monomer and for filaments of N units long this necessitates solving a set of 3^N coupled equations. We have however managed to obtain a solution for $j(c)$ by projecting the full system of 3^N equations to a set of just 3 exact equations for the return probabilities ψ_t^T, ψ_t^P , and ψ_t^D . These are the probabilities that a given monomer which was polymerized at $t = 0$ is again at the tip at time t as ATP-actin, ADP-Pi-actin, or ADP-actin, respectively. It is shown in the Appendix that $j(c)$ can be expressed in terms of their time integrals. As outlined in the Appendix, we then solved numerically these closed evolution equations for the return probabilities, leading to $j(c)$ of fig. 3(a). In addition to this method, we have also simulated the stochastic tip dynamics employing the Monte Carlo (MC) kinetic algorithm of Bortz, Kalos, and Lebowitz [32] to evolve the state of a filament tip in time and to calculate its mean growth rate. Each step of the algorithm entails updating time by an amount depending on the rate and number of possible future events, namely polymerization/depolymerization, hydrolysis, and phosphate release. These MC results fully agree with the numerical solutions of the closed equations, and in addition have provided us with the values for

Till now we have studied the simplest “one body” model, assuming on/off rates depend only on the attaching/detaching species [6]. Since a polymerizing or depolymerizing monomer makes or breaks bonds with two nearest neighbors each belonging to a different protofilament, clearly two and three body interactions also exist. Thus rates may also depend on the state of neighbors. We have studied many body effects using the MC method. Order unity changes in the shape of $j(c)$ below c^* result when order unity differences are introduced between many body rate constants which would have been identical in the one body model (results not shown). However, the essential picture of four distinct regions of behavior remains valid. Since a one body framework can adequately interpret existent growth rate curves (see fits to data in fig. 2) we do not explore these effects

further for the barbed end.

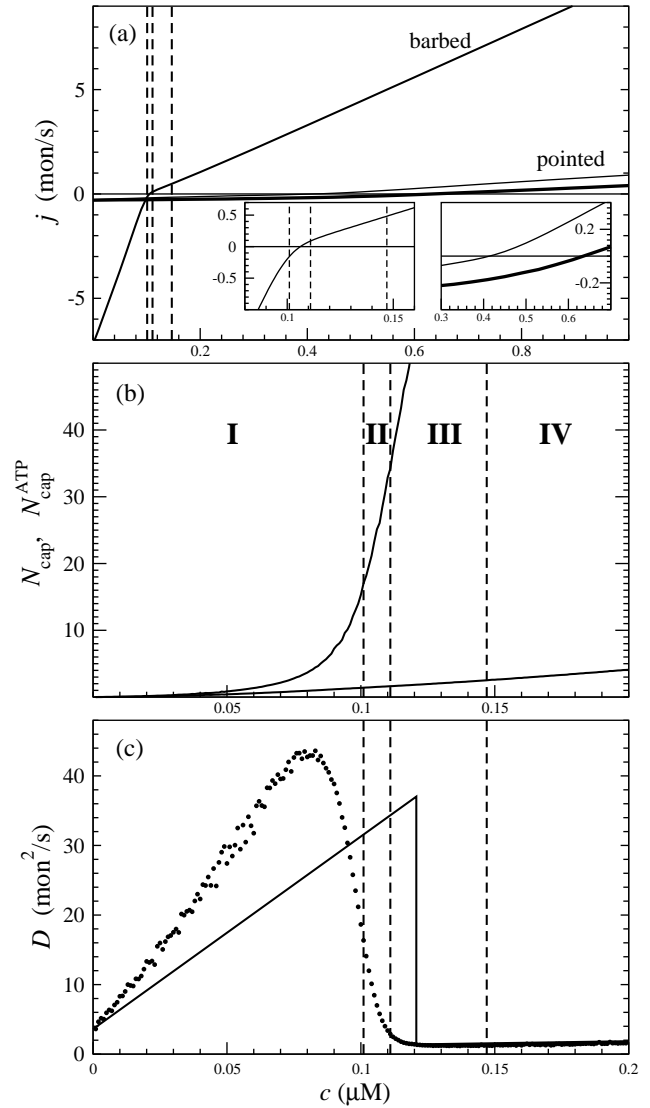


Figure 3: (a) Calculated growth rates $j(c)$. Results from numerical solutions and MC simulations are indistinguishable. See main text for parameter values. Pointed end: thick (thin) line shows many body (one body) model results. Insets exhibit critical region. Vertical dashed lines indicate $c_{\text{crit}} - \Delta c$, $c_{\text{crit}} + \Delta c$, c^* . They define 4 regions of behavior, I-IV (see main text). (b) MC results for N_{cap} (top curve) and $N_{\text{cap}}^{\text{ATP}}$ (bottom curve) at barbed end, same parameters as (a). (c) Length diffusion coefficient $D(c)$ at barbed end, MC results, same parameters as (a). Solid line: prediction of simplified model.

Pointed End $j(c)$: Why is c_{crit} so Different?

We will now assume the same mechanisms of random hydrolysis and slow phosphate release apply at the pointed end. Now an important issue in actin polymerization is how similar or dissimilar the ATP-actin and ADP-Pi-actin species are, in terms of on and off rate constants. That they are similar is suggested by the observation that excess phosphate reduces the critical concentration in a pure ADP-actin polymerization to a value rather close to the barbed end c_{crit} in ATP [11, 33, 34]. But if indeed the 2 species are similar, and the same basic mechanisms apply at the pointed end, this is inconsistent with the fact that

the critical concentration of ATP-actin (in the presence of Mg) is approximately 6 times that at the barbed end. This inconsistency follows from the cap structure, which includes a long ADP-Pi segment essentially hiding the ADP-actin core which is rarely seen at the filament tip (see fig. 1(a)). For the barbed end (fig. 3(b)) $N_{\text{cap}} \approx 25$ at c_{crit} , and we find the same is true for the pointed end, though not quite so long. Thus differences between ATP-actin and ADP-actin properties cannot account for the large c_{crit} difference between barbed and pointed end; we have verified this by calculating c_{crit} values which are weakly influenced by changing ADP-actin properties (not shown). Thus the origin must be different ATP-actin/ADP-Pi-actin compositions at the pointed and barbed ends; since the ATP-actin segment is short, $N_{\text{cap}}^{\text{ATP}} \approx 1$, both species are regularly exposed at filament ends and substantially different c_{crit} values will result provided the 2 species are distinct. Were they identical, c_{crit} at both ends would be very close to the value for a pure ATP-actin polymerization.

This leaves several possibilities. It may be that very different mechanisms operate during pointed end growth. It is also possible that differing properties of ATP-actin and ADP-Pi-actin are in fact consistent with the experiments of refs. 11, 33, 34 which may include addition of ADP-actin to growing filaments, as suggested by other studies indicating phosphate is only weakly bound to ADP-actin monomer [34]. In fact there is evidence favoring differences between the 2 species: the critical concentration of ATP-actin in excess phosphate is different at the two ends [11].

Adhering to the basic assumption of this work, that the growth mechanisms as previously outlined apply to both ends, we are led to the following conclusion: the values of c_{crit} for ATP-actin at both ends will be only weakly affected by the presence of excess phosphate (provided ionic conditions are strictly unchanged). This is because the binding of phosphate to ADP-actin segments is almost irrelevant since these are rarely exposed at the tip due to long caps in the critical regions. Indeed, for the barbed end no significant shift has been observed in the presence of phosphate [11, 33, 34]. For the pointed end, however, a reduction of c_{crit} has been reported in the presence of phosphate and barbed end capping proteins [11, 33, 34]. This cannot be explained within the present framework, and future experiment will hopefully settle this important issue.

the cap size as a function of c shown in fig. 3(b).

Can the proposed differences between the 2 species quantitatively account for the large c_{crit} of the pointed end? From ref. 6, $k_{\text{T}}^+ \approx 1.3\mu\text{M}^{-1}\text{s}^{-1}$ and $v_{\text{D}}^- \approx 0.27\text{s}^{-1}$. An important constraint in the one-body model is that the ratio $v_{\text{T}}^-/k_{\text{T}}^+$ must be identical at both ends for self-consistency. Thus, given the barbed end parameters of fig. 3(a), one is forced to choose $v_{\text{T}}^- = 0.16\text{s}^{-1}$ for the pointed end. The only unknown parameter is then v_{P}^- . We find that to account for the observed $c_{\text{crit}} \approx .6\mu\text{M}$ a very large value must be used $v_{\text{P}}^- = 8\text{s}^{-1}$. In fig. 3(a) we present the calculated $j(c)$ for the pointed end using a more realistic value $v_{\text{P}}^- = 2\text{s}^{-1}$ which gives $c_{\text{crit}} = .4\mu\text{M}$, and using $r_{\text{H}} = .3\text{s}^{-1}$, $r_{\text{P}_1} = .004\text{s}^{-1}$. Note that because v_{D}^- is close to v_{T}^- , slope changes are far less dramatic than for the barbed ends and regions I-IV hard to distinguish.

Our one body analysis suggests only high off rates of ADP-Pi-actin at the pointed end can explain the large c_{crit} . Given no current experimental evidence for this, could many body interactions be the explanation? In fact by varying many body parameters we were able to generate MC data with the correct c_{crit} value at the pointed end without assuming very large v_{P}^- . One example is shown in fig. 3(a) where the addition rate con-

stant is $1.3\mu\text{M}^{-1}\text{s}^{-1}$ onto an ATP-actin tip and $.2\mu\text{M}^{-1}\text{s}^{-1}$ onto any other tip type (other parameters unchanged from the one-body analysis above). In this case for $v_{\text{P}}^- \approx 0.4\text{s}^{-1}$ we obtain $c_{\text{crit}} \approx 0.6\mu\text{M}$. Future measurements of v_{P}^- at each end separately will help clarify if a one body description can account for the observed c_{crit} values or if many body effects must be invoked.

Fluctuations and Dynamical Instability

Turning now to fluctuations in growth rates, embodied in the length diffusivity D (see fig. 1(b)), we will see these behave dramatically around the critical region reflecting a mild version of the dynamical instability exhibited by microtubules [25, 35, 36]. As we did for mean growth rates, it will be helpful to first analyze fluctuations in the simplified 2-species model defined by assumptions (A) and (B) above.

The diffusivity D describes the random walk performed by the filament tip; if the tip makes a random forwards or backwards step of L monomer units every time interval T , then one can write $D = L^2/T$. Now just above the critical concentration, where the on and off rates are approximately equal, the tip randomly adds or subtracts one ATP-actin ($L = 1$) in a mean time $T = 1/v_{\text{T}}^-$, giving $D \approx v_{\text{T}}^- \equiv D_0$. Just below the critical concentration, however, there is a long steady state cap and changes in filament length are due to the occasional uncapping events (as in our discussion for $j(c)$) exposing the ADP core. These events are correlated on the timescale of the cap lifetime, the time taken by the tip to diffuse a distance of order the cap size, $t_{\text{cap}} \approx N_{\text{cap}}^2/D_0$. Thus one must take $T = t_{\text{cap}}$. Using a well known result from the theory of 1D random walks [25], the number of uncapping events during the cap lifetime is approximately $(D_0 t_{\text{cap}})^{1/2} \approx N_{\text{cap}}$. Since the number of core monomers lost during each uncapping episode before a polymerizing monomer arrives is of order $v_{\text{D}}^-/v_{\text{T}}^-$, thus $L = N_{\text{cap}} v_{\text{D}}^-/v_{\text{T}}^-$. This leads to a very different expression for the diffusivity, $D \approx (v_{\text{D}}^-)^2/v_{\text{T}}^-$: there is a discontinuity in diffusivity at c_{crit} of magnitude

$$\Delta D = D_0(\lambda^2 - 1), \quad \lambda \equiv v_{\text{D}}^-/v_{\text{T}}^-, \quad D_0 \equiv v_{\text{T}}^- . \quad (4)$$

At the barbed end the instability parameter $\lambda \approx 7$ and fluctuations at the critical concentration are very large, with a pronounced discontinuous drop in D as one passes to higher c . An exact derivation of eq. (4) reveals that the numerical prefactor is indeed unity while for concentrations away from the critical point one obtains the sawtooth curve in fig. 3(c) (details to be published). Notice that D decreases as concentrations become smaller since at $c = 0$ one must recover the Poissonian fluctuations of a pure depolymerization process for which $D = v_{\text{D}}^-/2$.

As for mean growth rates $j(c)$, the simplified model captures important features. When assumption (A) is undone, the large fluctuations at criticality remain but with renormalized diffusivity \tilde{D} and instability $\tilde{\lambda}$ and the discontinuity is shifted to the new c_{crit} location. Undoing assumption (B), phosphate release broadens the discontinuity in a region close to region II of half width Δc , similarly to its smoothing effect on the growth rate curve. This is seen in fig. 3(c), where we show MC results for diffusivity using the same values for the rate constants as for the barbed end in fig. 3(a). Note the shift in discontinuity position.

Can the results of fig. 3(c) explain the large fluctuations observed by Fujiwara et al. [27] and also suggested by the findings of ref. 37? Fig. 3(c) shows a peak value of $D \approx 45\text{mon}^2\text{s}^{-1}$, dropping to $D \approx 1\text{mon}^2\text{s}^{-1}$ above c_{crit} whereas

$D = 25 - 29 \text{mon}^2 \text{s}^{-1}$ was reported in the experiments. However, these measurements were performed at steady state where overall filament elongation rate is zero, i.e. at a concentration slightly above c_{crit} for the barbed end and well below that for the pointed, corresponding to a theoretical value less than $D = 5 \text{mon}^2 \text{s}^{-1}$. We suggest that large length fluctuations due to dynamical instability of a monomer-by-monomer growth process may underlie these experiments, however it may be than an entirely different physical mechanism is involved. Measurements of the full $D(c)$ curve will help clarify this fundamental question. Our work leads also to the following predictions: (i) since phosphate will bind to ADP-actin and eliminate the effect of a large instability parameter $\tilde{\lambda}$, thus fluctuations and D at the barbed end will be suppressed in the presence of excess phosphate and (ii) fluctuations at the pointed end are much smaller in magnitude since v_{D}^- is small at this end.

Discussion

In this work we modeled actin polymerization kinetics based on the assumptions of irreversible random ATP hydrolysis and random phosphate release. Filament growth rates $j(c)$ and their fluctuations, as measured by the diffusivity $D(c)$, were calculated as functions of monomeric ATP-actin concentration c . We showed quantitatively how the composition and dynamics of the ATP-actin and ADP-Pi-caps is reflected in these observables. To our knowledge, this is the first rigorous calculation of these quantities accounting for the above basic mechanisms. In a related study Pantaloni et al. [23, 24] have studied $j(c)$ at the barbed end in a work which was formulated before the mechanism of phosphate release was discovered. Infinitely fast phosphate release and vectorial hydrolysis were assumed. Given the data available at that time, in order to explain the sharp change in slope of $j(c)$ between regions I and IV in fig. 3(a), they had to further assume (i) strong three body ATP-actin/ADP-actin interactions which lead to stable short ATP-actin caps, and (ii) zero hydrolysis rate of the terminal nucleotide bound to the monomer at the tip. In our work, the origin of the sharp change in slope is precisely the fact that phosphate release is slow, similarly to an earlier model of microtubule polymerization [38].

In an interesting new work Bindschadler et al. [26] studied the composition of actin filaments accounting for all three actin species. In their work a preaveraging approximation was implicitly used: the probability to find a given nucleotide sequence along the filament was assumed to be equal to products of probabilities. Even though determining the growth rate as a function of c was not the objective of their work, it can be shown that preaveraging generates different $j(c)$ curves to ours since it does not correctly capture correlations and fluctuations. Another difference relative to our study is that these workers considered a one body model with identical ATP-actin and ADP-Pi-actin rate constants ($v_{\text{T}}^- = v_{\text{P}}^-$), but the ratio $v_{\text{T}}^-/k_{\text{T}}^+$ was taken to be different at the two ends.

Here we have addressed random ATP hydrolysis only. Future work is needed to analyze the implications of the vectorial hydrolysis suggested by refs. 14, 23. We showed that for random hydrolysis $j(c)$ is linear far above the critical concentration (region IV in fig. 3). Growth rate experiments for both ends together in the absence of KCl have exhibited nonlinearities up to $c = 10 \mu\text{M}$, far above the critical concentration of the barbed end which is $1 \mu\text{M}$ under these conditions [4, 5]. In refs. 4, 23 this observation was attributed to vectorial hydrolysis at the barbed end while in ref. 6 this was assigned to the non-linear contribution of the pointed end whose critical concentration is $\approx 5 \mu\text{M}$ under the same conditions.

Perhaps our most interesting finding is that D has a large peak at the critical concentration c_{crit} of the barbed end, fol-

lowed by a sharp drop in a narrow concentration range above c_{crit} . This conclusion is quite general, independent of detailed values of rate constants. Its origin is the smallness of the phosphate release rate and the large value of v_{D}^- at the barbed end, and it can be shown to remain valid even if a vectorial hydrolysis mechanism is assumed. To the best of our knowledge no experiments have yet measured length diffusivities over a range of concentrations. These promise to provide new information and insight on the fundamentals of actin polymerization.

This work was supported by the Petroleum Research Fund under grant no. 33944-AC7 and NSF under grant no. CHE-00-91460. We thank Thomas Pollard for stimulating discussions.

Appendix: Numerical algorithm for Growth Rate

For $j < 0$ the growth rate is related to the return probabilities by $j = v_{\text{D}}^- p_{\text{core}}$, where $p_{\text{core}} = 1 - \int_0^\infty dt (\psi_t^{\text{D}} + \psi_t^{\text{P}} + \psi_t^{\text{T}})$ is the probability of exposure of the ADP-actin core at the tip. For $j > 0$ one has $j = k_{\text{T}}^+ c - \int_0^\infty dt F_t$ where $F_t \equiv \psi_t^{\text{T}} v_{\text{T}}^- + \psi_t^{\text{P}} v_{\text{P}}^- + \psi_t^{\text{D}} v_{\text{D}}^-$ is the depolymerization rate at time t of a monomer which added to the tip at $t = 0$. The integral of F_t is the total depolymerization rate of added monomers. In the supporting material we present the dynamical equations obeyed by the return probabilities. We found the Laplace transform of the latter, $t \rightarrow E$ and $F \rightarrow f$, leads to a closed recursive equation relating f_E to $f_{E+r_{\text{H}}}$ and $f_{E+r_{\text{P}}}$. With boundary condition $f_E \rightarrow 0$ as $E \rightarrow \infty$, we started from large E values and evolved this equation numerically towards $E = 0$ to obtain $f_0 = \int_0^\infty dt F_t$. Given this, the time integrals of the return probabilities can be directly obtained from the dynamical equations and j can be subsequently determined.

References

- [1] Shterline, P, Clayton, J, & Sparrow, J. C. (1998) *Actin*. (Oxford University Press, New York).
- [2] Pollard, T. D & Borisy, G. G. (2003) *Cell* **112**, 453–465.
- [3] Korn, E. D, Carlier, M.-F, & Pantaloni, D. (1987) *Science* **238**, 638–643.
- [4] Carlier, M.-F, Pantaloni, D, & Korn, E. D. (1984) *J. Biol. Chem.* **259**, 9983–9986.
- [5] Carlier, M.-F, Pantaloni, D, & Korn, E. D. (1985) *J. Biol. Chem.* **260**, 6565–6571.
- [6] Pollard, T. D. (1986) *J. Cell Biol.* **103**, 2747–2754.
- [7] Coué, M & Korn, E. D. (1986) *J. Biol. Chem.* **261**, 1588–1593.
- [8] Carlier, M.-F, Criquelet, P, Pantaloni, D, & Korn, E. D. (1986) *J. Biol. Chem.* **261**, 2041–2050.
- [9] Carlier, M.-F, Pantaloni, D, & Korn, E. D. (1986) *J. Biol. Chem.* **261**, 10785–10792.
- [10] Weber, A, Northrop, J, Bishop, M. F, Ferrone, F. A, & Mooseker, M. S. (1987) *Biochemistry* **26**, 2537–2544.
- [11] Carlier, M.-F & Pantaloni, D. (1988) *J. Biol. Chem.* **263**, 817–825.
- [12] Pardee, J. D & Spudich, J. A. (1982) *J. Cell Biol.* **93**, 648–654.
- [13] Pollard, T. D & Weeds, A. G. (1984) *FEBS Lett.* **170**, 94–98.
- [14] Carlier, M.-F, Pantaloni, D, & Korn, E. D. (1987) *J. Biol. Chem.* **262**, 3052–3059.
- [15] Ohm, T & Wegner, A. (1994) *Biochim. Biophys. Acta* **1208**, 8–14.
- [16] Pieper, U & Wegner, A. (1996) *Biochemistry* **35**, 4396–4402.
- [17] Blanchoin, L & Pollard, T. D. (2002) *Biochemistry* **41**, 597–602.
- [18] Carlier, M.-F & Pantaloni, D. (1986) *Biochemistry* **35**, 7789–7792.
- [19] Carlier, M.-F. (1987) *Biochemical and Biophysical Research Communications* **143**, 1069–1075.
- [20] Melki, R, Fievez, S, & Carlier, M.-F. (1996) *Biochemistry* **35**, 12038–12045.
- [21] Amann, K. J & Pollard, T. D. (2001) *Proc. Natl. Acad. Sci. USA* **98**, 15009–15013.

- [22] Ichetovkin, I, Grant, W, & Condeelis, J. (2002) *Curr. Biol.* **12**, 79–84.
- [23] Pantaloni, D, Hill, T. L, Carlier, M. F, & Korn, E. D. (1985) *Proc. Natl. Acad. Sci. USA* **82**, 7207–7211.
- [24] Hill, T. L. (1986) *Biophys. J.* **49**, 981–986.
- [25] Hill, T. L. (1987) *Linear Aggregation Theory in Cell Biology*. (Springer Verlag, New York).
- [26] Bindschadler, M, Osborn, E. A, Dewey, C. F. J, & McGrath, J. L. (2004) (*preprint*).
- [27] Fujiwara, I, Takahashi, S, Takaduma, H, Funatsu, T, & Ishiwata, S. (2002) *Nature Cell Biology* **4**, 666–673.
- [28] O’Shaughnessy, B & Vavylonis, D. (2003) *Phys. Rev. Lett.* **90**, 118301.
- [29] O’Shaughnessy, B & Vavylonis, D. (2003) *Eur. Phys. J. E* **12**, 481–496.
- [30] Littlefield, R & Fowler, V. M. (2002) *Nature Cell Biology* **4**, E209–E210.
- [31] Kinoshian, H. J, Selden, L. A, Estes, J. E, & Gershman, L. C. (1993) *J. Biol. Chem.* **268**, 8683–8691.
- [32] Bortz, A. B, Kalos, M. H, & Lebowitz, J. L. (1975) *Journal of Computational Physics* **17**, 10–18.
- [33] Rickard, J. E & Sheterline, P. (1986) *J. Mol. Biol.* **191**, 273–280.
- [34] Wanger, M & Wegner, A. (1987) *Biochimica et Biophysica Acta* **915**, 105–113.
- [35] Mitchison, T & Kirschner, M. (1984) *Nature* **312**, 237–242.
- [36] Hill, T. L & Chen, Y.-D. (1984) *Proc. Natl. Acad. Sci. USA* **81**, 5772–5776.
- [37] Brenner, S. L & Korn, E. D. (1983) *J. Biol. Chem.* **258**, 5013–5020.
- [38] Hill, T. L & Carlier, M.-F. (1983) *Proc. Natl. Acad. Sci. USA* **80**, 7234–7238.

SUPPORTING MATERIAL

In this supporting material we describe the numerical method we used in the main text to calculate the growth rate curves of figs. 2 and 3(a). Consider an ATP-actin monomer which polymerizes at the filament tip at time $t = 0$. We define the return probabilities ψ_t^T , ψ_t^P , and ψ_t^D to be the probability that this monomer is once again at the tip after time t as ATP-actin, ADP-Pi-actin, or ADP-actin, respectively. The total depolymerization rate of this monomer at time t is

$$F_t = v_{\text{T}}^- \psi_t^T + v_{\text{P}}^- \psi_t^P + v_{\text{D}}^- \psi_t^D . \quad (5)$$

The dynamical equations obeyed by the return probabilities are

$$\begin{aligned} \frac{d}{dt} \psi_t^T &= -(k_{\text{T}}^+ c + v_{\text{T}}^- + r_{\text{H}}) \psi_t^T + k_{\text{T}}^+ c \int_0^t dt' \psi_{t-t'}^T F_{t-t'} e^{-r_{\text{H}}(t-t')} , \\ \frac{d}{dt} \psi_t^P &= -(k_{\text{T}}^+ c + v_{\text{P}}^- + r_{\text{Pi}}) \psi_t^P + r_{\text{H}} \psi_t^T + k_{\text{T}}^+ c \int_0^t dt' \psi_{t-t'}^P F_{t-t'} e^{-r_{\text{Pi}}(t-t')} \\ &\quad + k_{\text{T}}^+ c \int_0^t dt' \psi_{t-t'}^T F_{t-t'} \frac{r_{\text{H}}}{r_{\text{Pi}} - r_{\text{H}}} \left(e^{-r_{\text{H}}(t-t')} - e^{-r_{\text{Pi}}(t-t')} \right) , \\ \frac{d}{dt} \psi_t^D &= -(k_{\text{T}}^+ c + v_{\text{D}}^-) \psi_t^D + r_{\text{Pi}} \psi_t^P + k_{\text{T}}^+ c \int_0^t dt' \psi_{t-t'}^D F_{t-t'} + k_{\text{T}}^+ c \int_0^t dt' \psi_{t-t'}^P F_{t-t'} \left(1 - e^{-r_{\text{Pi}}(t-t')} \right) \\ &\quad + k_{\text{T}}^+ c \int_0^t dt' \psi_{t-t'}^T F_{t-t'} \left(1 - \frac{r_{\text{Pi}}}{r_{\text{Pi}} - r_{\text{H}}} e^{-r_{\text{Pi}}(t-t')} + \frac{r_{\text{H}}}{r_{\text{Pi}} - r_{\text{H}}} e^{-r_{\text{Pi}}(t-t')} \right) . \end{aligned} \quad (6)$$

Here the non-integral terms on the right hand sides represent change of tip status due to polymerization, depolymerization, hydrolysis, and phosphate release events at time t . The integral terms represent rates of reappearance of the monomer at the tip, weighted by factors accounting for the probability of hydrolysis or phosphate release during the time interval since the last appearance at the tip. For example, the first term on the right hand side of the first equation represents the rate of change of the probability of finding the ATP-actin monomer at the tip due to (i) polymerization of another monomer on top of it, (ii) depolymerization of the monomer itself, or (iii) hydrolysis of the ATP nucleotide bound to the monomer at the tip. The integral term on the right hand side represents reappearance events of the ATP-actin unit at the tip given that it got buried inside the filament due to a polymerization event at time t' , an event which occurred with rate $k_{\text{T}}^+ c$. Factor F represents the rate of reappearance of the buried monomer at the tip due to depolymerization of all the monomers which were added on top of it. Factor $e^{-r_{\text{H}}(t-t')}$ is the probability that the ATP-actin monomer in question is not hydrolyzed while being buried.

Now as discussed in the Appendix, the filament growth rate is given by

$$j = \begin{cases} v_{\text{D}}^- [1 - \int_0^\infty dt (\psi_t^D + \psi_t^P + \psi_t^T)] & (j < 0) \\ k_{\text{T}}^+ c - \int_0^\infty dt F_t & (j > 0) \end{cases} \quad (7)$$

Carrying out a Laplace transformation, $t \rightarrow E$, $F_t \rightarrow f_E$, and $\psi_t \rightarrow \Psi_E$ one has from eq. (7)

$$j = \begin{cases} v_{\text{D}}^- [1 - \Psi_0^D - \Psi_0^P - \Psi_0^T] & (j < 0) \\ k_{\text{T}}^+ c - f_0 & (j > 0) \end{cases} \quad (8)$$

while from eq. (6) one obtains

$$\begin{aligned} \Psi_E^T &= 1 / (E + v_{\text{T}}^- + r_{\text{H}} + k_{\text{T}}^+ c(1 - f_{E+r_{\text{H}}})) , \\ \Psi_E^P &= \frac{r_{\text{H}} + k_{\text{T}}^+ c r_{\text{H}}(f_{E+r_{\text{H}}} - f_{E+r_{\text{Pi}}}) / (r_{\text{Pi}} - r_{\text{H}})}{E + v_{\text{P}}^- + r_{\text{Pi}} + k_{\text{T}}^+ c(1 - f_{E+r_{\text{Pi}}})} \Psi_E^T , \\ \Psi_E^D &= \frac{(r_{\text{Pi}} + k_{\text{T}}^+ c(f_E - f_{E+r_{\text{Pi}}})) \Psi_E^P + k_{\text{T}}^+ c(f_E - r_{\text{Pi}} f_{E+r_{\text{H}}}) / (r_{\text{Pi}} - r_{\text{H}}) + r_{\text{H}} f_{E+r_{\text{Pi}}} / (r_{\text{Pi}} - r_{\text{H}})}{E + v_{\text{D}}^- + k_{\text{T}}^+ c(1 - f_E)} \Psi_E^T . \end{aligned} \quad (9)$$

Eliminating all Ψ in the Laplace transformation of eq. (5) after using eq. (9) one obtains the following recursive relationship involving the function f alone:

$$f_E = \mathcal{R}[f_{E+r_{\text{H}}}, f_{E+r_{\text{Pi}}}] , \quad (10)$$

where

$$\mathcal{R}[f_{E+r_{\text{H}}}, f_{E+r_{\text{Pi}}}] = \frac{-b_1 + \sqrt{b_1^2 - 4b_2 b_0}}{2b_2} . \quad (11)$$

Here the symbols b_0 , b_1 , and b_2 are functions of E , f_{E+r_H} and $f_{E+r_{P_i}}$ as follows:

$$\begin{aligned}
b_0 &= A_{0,2}E^2 + A_{0,1}E + A_{0,0} , \\
b_1 &= A_{1,3}E^3 + A_{1,2}E^2 + A_{1,1}E + A_{1,0} , \\
b_2 &= A_{2,2}E^2 + A_{2,1}E + A_{2,0} ,
\end{aligned} \tag{12}$$

where

$$\begin{aligned}
A_{0,2} &= -(r_H - r_{P_i})v_T^- k_T^+ c , \\
A_{0,1} &= (v_D^- r_H - r_{P_i}v_T^- + r_H(-v_P^- + v_T^-))(k_T^+ c)^2 f_{E+r_{P_i}} + (r_H v_P^- - v_D^- r_{P_i})(k_T^+ c)^2 f_{E+r_H} \\
&\quad - (r_H - r_{P_i})k_T^+ c(r_H v_P^- + v_T^-(v_D^- + v_P^- + r_{P_i} + 2k_T^+ c)) , \\
A_{0,0} &= -v_D^-(r_H - r_{P_i})(k_T^+ c)^3 f_{E+r_{P_i}} f_{E+r_H} \\
&\quad - (r_H(v_P^- - v_T^-) + r_{P_i}v_T^-)k_T^+ c + v_D^-((r_H)^2 - r_{P_i}v_T^- + r_H(-r_{P_i} + v_T^- + k_T^+ c))(k_T^+ c)^2 f_{E+r_{P_i}} \\
&\quad + (r_H v_P^- k_T^+ c + v_D^-(r_H(v_P^- + r_{P_i}) - r_{P_i}(v_P^- + r_{P_i} + k_T^+ c)))(k_T^+ c)^2 f_{E+r_H} \\
&\quad - (r_H - r_{P_i})k_T^+ c(k_T^+ c(r_H v_P^- + v_T^-(v_P^- + r_{P_i} + k_T^+ c)) + v_D^-(r_H(v_P^- + r_{P_i}) + v_T^-(v_P^- + r_{P_i} + k_T^+ c))) , \\
A_{1,3} &= r_H - r_{P_i} , \\
A_{1,2} &= -(r_H - r_{P_i})k_T^+ c(f_{E+r_{P_i}} + f_{E+r_H}) + (r_H - r_{P_i})(v_D^- + r_H + v_P^- + r_{P_i} + v_T^- + 3k_T^+ c) , \\
A_{1,1} &= (r_H - r_{P_i})(k_T^+ c)^2 f_{E+r_{P_i}} f_{E+r_H} - (r_H - r_{P_i})(v_D^- + r_H + v_T^- + 2k_T^+ c)k_T^+ c f_{E+r_{P_i}} \\
&\quad - (r_H - r_{P_i})(v_D^- + v_P^- + r_{P_i} + 2k_T^+ c)k_T^+ c f_{E+r_H} \\
&\quad + (r_H - r_{P_i})(v_P^- v_T^- + r_{P_i}v_T^- + 2v_P^- k_T^+ c + 2r_{P_i}k_T^+ c + 3v_T^- k_T^+ c + 3(k_T^+ c)^2 \\
&\quad \quad + v_D^-(r_H + v_P^- + r_{P_i} + v_T^- + k_T^+ c) + r_H(v_P^- + r_{P_i} + 2k_T^+ c)) , \\
A_{1,0} &= (r_H - r_{P_i})(v_D^- + k_T^+ c)(k_T^+ c)^2 f_{E+r_{P_i}} f_{E+r_H} \\
&\quad + (-v_D^-(r_H^2 - r_{P_i}v_T^- + r_H(-r_{P_i} + v_T^- + k_T^+ c)) \\
&\quad \quad + k_T^+ c(-r_H^2 + r_H(v_P^- + r_{P_i} - 2v_T^- - k_T^+ c) + r_{P_i}(2v_T^- + k_T^+ c)))k_T^+ c f_{E+r_{P_i}} \\
&\quad + (v_D^-(-r_H(v_P^- + r_{P_i}) + r_{P_i}(v_P^- + r_{P_i} + k_T^+ c)) \\
&\quad \quad + k_T^+ c(r_{P_i}(v_P^- + r_{P_i} + k_T^+ c) - r_H(2v_P^- + r_{P_i} + k_T^+ c)))k_T^+ c f_{E+r_H} \\
&\quad + (r_H - r_{P_i})(v_D^-(r_H(v_P^- + r_{P_i}) + v_T^-(v_P^- + r_{P_i} + k_T^+ c)) \\
&\quad \quad + k_T^+ c(r_H(2v_P^- + r_{P_i} + k_T^+ c) + (v_P^- + r_{P_i} + k_T^+ c)(2v_T^- + k_T^+ c))) , \\
A_{2,2} &= r_{P_i} - r_H , \\
A_{2,1} &= (r_H - r_{P_i})k_T^+ c(f_{E+r_{P_i}} + f_{E+r_H}) - (r_H - r_{P_i})(r_H + v_P^- + r_{P_i} + v_T^- + 2k_T^+ c) , \\
A_{2,0} &= -(r_H - r_{P_i})(k_T^+ c)^2 f_{E+r_{P_i}} f_{E+r_H} + (r_H - r_{P_i})(r_H + v_T^- + k_T^+ c)k_T^+ c f_{E+r_{P_i}} \\
&\quad + (r_H - r_{P_i})(v_P^- + r_{P_i} + k_T^+ c)k_T^+ c f_{E+r_H} - (r_H - r_{P_i})(v_P^- + r_{P_i} + k_T^+ c)(r_H + v_T^- + k_T^+ c) .
\end{aligned} \tag{13}$$

We remark that eq. (11) is the solution of a quadratic equation; which of the two solutions of the quadratic is meaningful is easily checked by demanding $f < 1$ in the $E \rightarrow \infty$ limit.

Now for any given monomer concentration c , with the boundary condition $f_E \rightarrow 0$ as $E \rightarrow \infty$, we started from a large enough E value and evolved eq. (10) towards $E = 0$ to obtain f_0 , $f_{r_{P_i}}$, and f_{r_H} . Substituting these values in eq. (9) we further obtained Ψ_0^T , Ψ_0^P and Ψ_0^D . Thus, given f_0 , Ψ_0^T , Ψ_0^P and Ψ_0^D we evaluated $j(c)$ using eq. (8). It was shown that this method converges to a unique solution provided one starts the evolution from large enough E , retaining a sufficient number of significant digits.